Inorganic Chemistry

including bioinorganic chemistry

November 18, 2013
Volume 52, Number 22
pubs.acs.org/IC

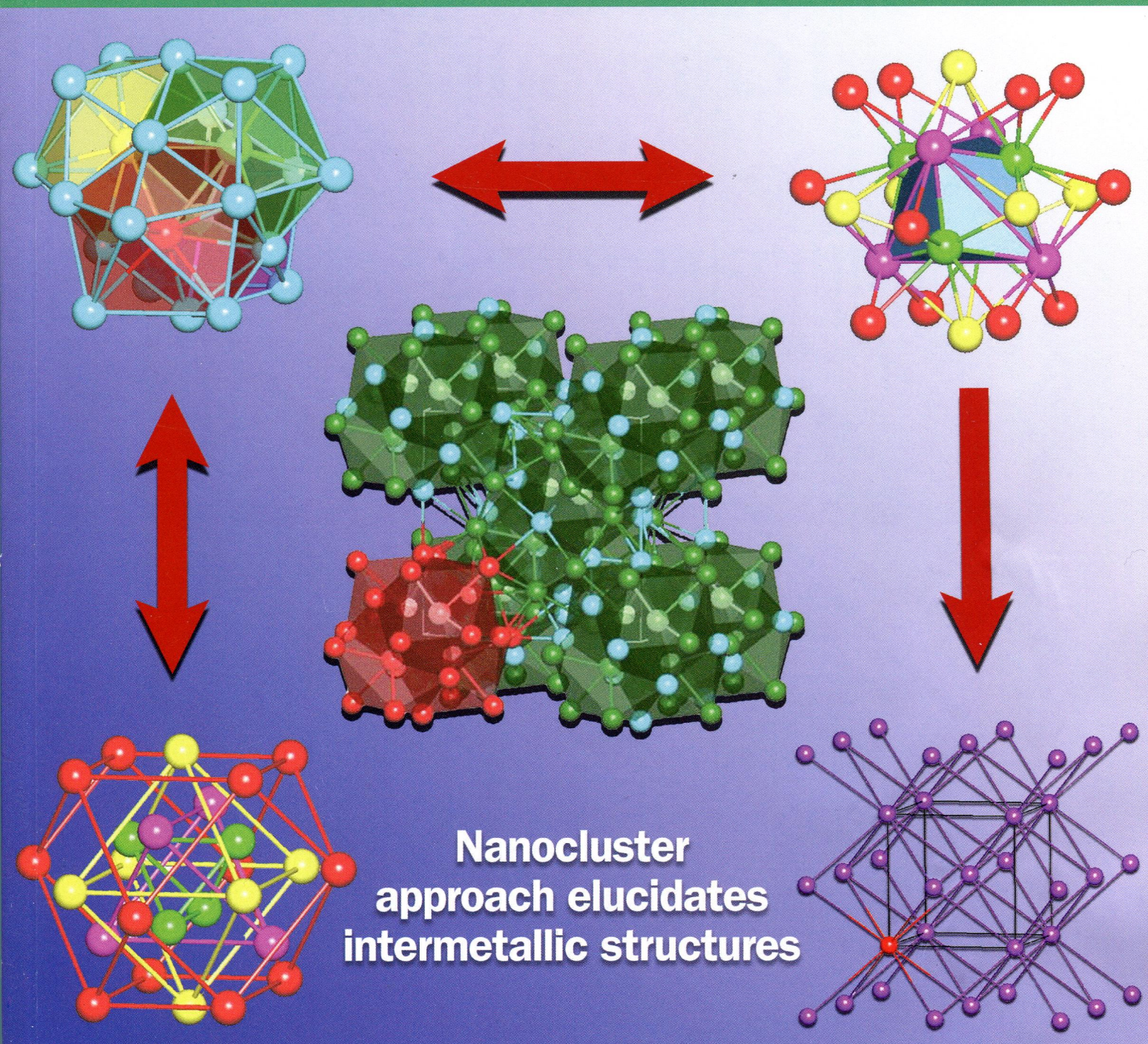

Nanocluster approach elucidates intermetallic structures

ACS Publications
MOST TRUSTED. MOST CITED. MOST READ.

www.acs.org

Inorganic Chemistry

NOVEMBER 18, 2013
VOLUME 52 ISSUE 22

INOCAJ 52(22) 12855−13288 (2013)
ISSN 0020-1669
Registered in the U.S. Patent and Trademark Office

ON THE COVER: Using a recently developed nanocluster approach, 26-atom nanoclusters of the γ-brass type were found in 5918 crystal structures of cubic intermetallics. The regularities in the chemical composition of the nanoclusters are revealed and analyzed. See A. A. Pankova, V. A. Blatov, G. D. Ilyushin, and D. M. Proserpio, p 13094.

Editorial

Communications

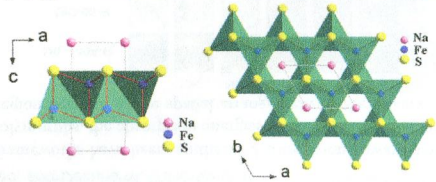

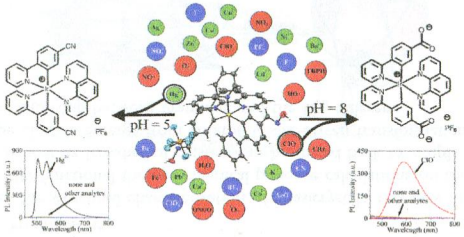

12866 S dx.doi.org/10.1021/ic402095u

Third-Generation Breathing Metal–Organic Framework with Selective, Stepwise, Reversible, and Hysteretic Adsorption Properties

Suresh Sanda, Srinivasulu Parshamoni, and Sanjit Konar*

A breathing metal–organic framework (MOF) shows reversible and stepwise adsorption toward a large number of adsorbates like CO_2 gas and MeOH, H_2O, and CH_3CN vapors. Desorption and adsorption processes involve unusual contraction and expansion and demonstrate the ability of the MOF to expand or shrink in the presence of external stimuli.

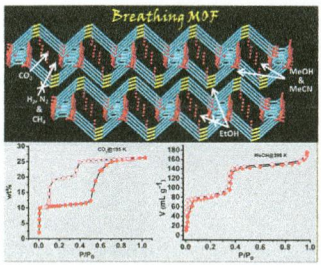

12869 S dx.doi.org/10.1021/ic402042e

Spin-Relaxation Properties of a High-Spin Mononuclear $Mn^{III}O_6$-Containing Complex

Alexios Grigoropoulos, Michael Pissas, Patroklos Papatolis, Vassilis Psycharis, Panayotis Kyritsis,* and Yiannis Sanakis*

The magnetic properties of the mononuclear manganese(III) complex $[Mn\{(OPPh_2)_2N\}_3]$ are investigated by means of magnetometry and dual-mode X-band electron paramagnetic resonance spectroscopy. The MnO_6 core exhibits tetragonal elongation due to Jahn–Teller distortions, resulting in negative zero-field splitting. Slow relaxation of magnetization, monitored by alternating-current magnetic susceptibility measurements, is induced in the presence of external magnetic fields.

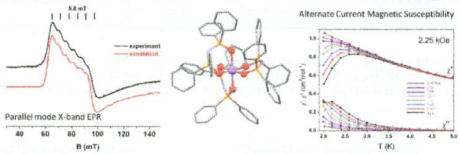

12872 S dx.doi.org/10.1021/ic402357u

Correlation of the Electronic and Geometric Structures in Mononuclear Copper(II) Superoxide Complexes

Jake W. Ginsbach, Ryan L. Peterson, Ryan E. Cowley, Kenneth D. Karlin,* and Edward I. Solomon*

Magnetic circular dichroism and ^2H NMR spectroscopy indicate that the end-on copper(II) superoxide complex $(HIPT_3tren)Cu^{II}O_2^{\bullet-}$ has a triplet ground state. This provides further evidence that the geometric structure of copper superoxide species controls their electronic structure.

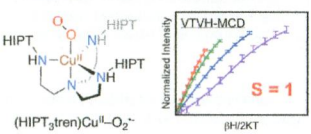

12875 Ⓢ dx.doi.org/10.1021/ic402412k

Problem Solving with Pentagons: Tsai-Type Quasicrystal as a Structural Response to Chemical Pressure

Veronica M. Berns and Daniel C. Fredrickson*

Even after significant advances in the structural characterization of quasicrystals, this new form of long-range order remains enigmatic. Here, we present density functional theory–chemical pressure calculations on the 1:1 Tsai-type quasicrystal approximant $CaCd_6$, which reveal how its icosahedral clusters can be traced back to simple $CaCu_5$-type intermetallics. The results indicate that the Tsai-type clusters emerge from an atomic-size-driven transformation from planar arrangements to spherical clusters, recalling the relationship between graphene and the C_{60} fullerene.

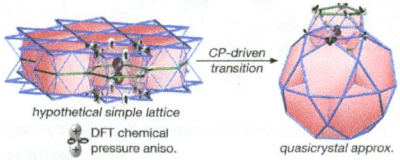

12878 Ⓢ dx.doi.org/10.1021/ic4024234

Microwave-Assisted Solvothermal Synthesis and Optical Properties of Tagged MIL-140A Metal–Organic Frameworks

Weibin Liang, Ravichandar Babarao, and Deanna M. D'Alessandro*

A series of tagged MIL-140A-R frameworks have been synthesized using a microwave-assisted solvothermal method. Compared with their UiO-66-R polymorphs, the absorption energies in the MIL-140A-R series (R = NH_2, NO_2, Br, Cl, and F) are extended toward the visible region because of the spatial arrangement of the linkers.

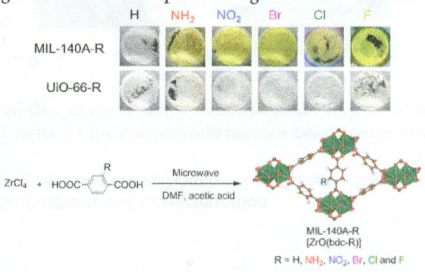

Articles

12881 S dx.doi.org/10.1021/ic400345w

Syntheses, Structures, Magnetic Properties, and Density Functional Theory Magneto-Structural Correlations of Bis(μ-phenoxo) and Bis(μ-phenoxo)-μ-acetate/Bis(μ-phenoxo)-bis(μ-acetate) Dinuclear $Fe^{III}Ni^{II}$ Compounds

Susanta Hazra, Sagarika Bhattacharya, Mukesh Kumar Singh, Luca Carrella, Eva Rentschler, Thomas Weyhermueller, Gopalan Rajaraman,* and Sasankasekhar Mohanta*

This report deals with the syntheses, crystal structures, and magnetic properties of a bis(μ-phenoxo) and a bis(μ-phenoxo)-μ-acetate/bis(μ-phenoxo)-bis(μ-acetate) dinuclear macrocyclic $Fe^{III}Ni^{II}$ compound, along with DFT modeling of the magnetic properties of these compounds and related compounds, accompanied by DFT-computed magneto-structural correlations.

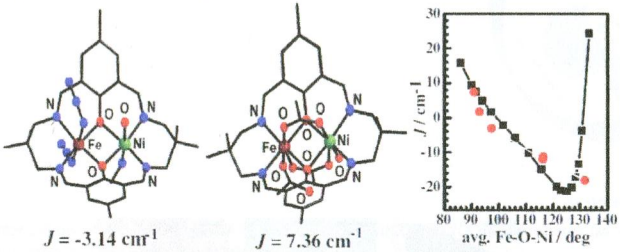

12893 S dx.doi.org/10.1021/ic400508y

Incorporation of Trinuclear Lanthanide(III) Hydroxo Bridged Clusters in Macrocyclic Frameworks

Michał J. Kobyłka, Katarzyna Ślepokura, Maria Acebrón Rodicio, Marta Paluch, and Jerzy Lisowski*

Chiral amine macrocycles derived from diformylphenols and *trans*-1,2-diaminocyclohexane form enantiopure trinuclear lanthanide(III) complexes, where a $Ln_3(\mu_3\text{-}OH)_2$ cluster is coordinated in the center of the macrocycle.

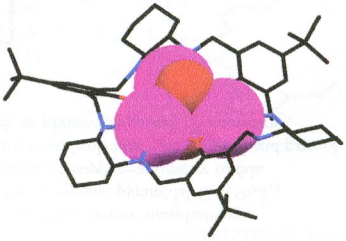

12904 S dx.doi.org/10.1021/ic4008203

The Protonation States of Oxo-Bridged Mn^{IV} Dimers Resolved by Experimental and Computational Mn K Pre-Edge X-ray Absorption Spectroscopy

Vera Krewald, Benedikt Lassalle-Kaiser, Thaddeus T. Boron III, Christopher J. Pollock, Jan Kern, Martha A. Beckwith, Vittal K. Yachandra, Vincent L. Pecoraro,* Junko Yano,* Frank Neese,* and Serena DeBeer*

A combined experimental and theoretical protocol for the determination of oxo bridge protonation states is established by the systematic investigation of the $[Mn^{IV}_2(salpn)_2(\mu\text{-}OH_n)_2]^{n+}$ series by experimental and computational Mn K pre-edge X-ray absorption spectroscopy. A TD-DFT approach for calculating the pre-edge spectra of molecules with multiple metal centers is presented, using both high spin (HS) and broken symmetry (BS) electronic structure solutions.

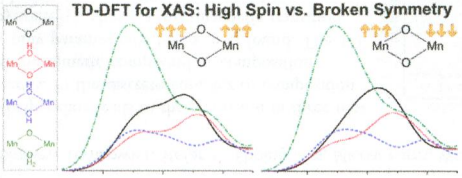

12915 S dx.doi.org/10.1021/ic400821g

Experimental and Computational X-ray Emission Spectroscopy as a Direct Probe of Protonation States in Oxo-Bridged Mn^{IV} Dimers Relevant to Redox-Active Metalloproteins

Benedikt Lassalle-Kaiser, Thaddeus T. Boron III, Vera Krewald, Jan Kern, Martha A. Beckwith, Mario U. Delgado-Jaime, Henning Schroeder, Roberto Alonso-Mori, Dennis Nordlund, Tsu-Chien Weng, Dimosthenis Sokaras, Frank Neese, Uwe Bergmann, Vittal K. Yachandra, Serena DeBeer,* Vincent L. Pecoraro,* and Junko Yano*

The valence-to-core X-ray emission spectra of the $[Mn^{IV}_2(salpn)_2(\mu\text{-}OH_n)_2]^{n+}$ series show significant changes in intensity and peak position upon oxo-bridge protonation, where specifically the satellite Kβ'' peak provides a direct signature of the protonation state change. DFT calculations were performed to simulate the valence-to-core XES spectra and to assign the spectral features to specific transitions.

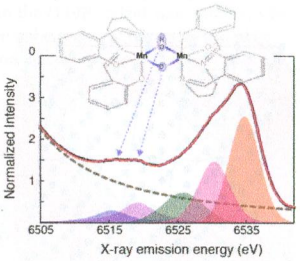

12923 S dx.doi.org/10.1021/ic400712s

Dividing the Spoils: Role of Pyrazine Ligands and Perchlorate Counterions in the Magnetic Properties of Bis(pyrazine) diperchloratecopper(II), $[Cu(pz)_2](ClO_4)_2$

Sergi Vela, Joaquim Jornet-Somoza, Mark M. Turnbull, Ralf Feyerherm, Juan J. Novoa, and Mercè Deumal*

A first-principles bottom-up computational study of $[Cu(pz)_2](ClO_4)_2$ shows a remarkable agreement in the whole range of temperatures between simulated and experimental magnetic susceptibility and heat capacity data. The antiferromagnetic behavior of $[Cu(pz)_2](ClO_4)_2$ is due to a 2D antiferromagnetic topology. The role of pyrazine ligands, perchlorate counterions, and hydrogen bonding is explored in order to interpret, and ultimately to be able to tune, the J_{AB} exchange coupling interactions between radicals.

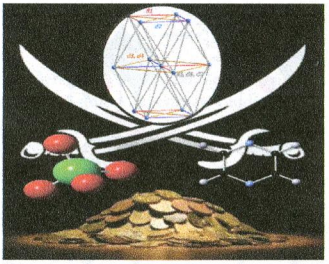

12933 S dx.doi.org/10.1021/ic401250d

The Influence of Heme Ruffling on Spin Densities in Ferricytochromes *c* Probed by Heme Core ^{13}C NMR

Jesse G. Kleingardner, Sarah E. J. Bowman, and Kara L. Bren*

NMR spectroscopy reveals the effects of heme ruffling on the distribution of spin density on low-spin ferric heme. Increased ruffling is correlated with lower spin densities on the β-pyrrole carbons and higher spin densities on the α-pyrrole carbons and meso carbons. Increased ruffling also is correlated with enhanced bonding between Fe(III) and the axial His ligand.

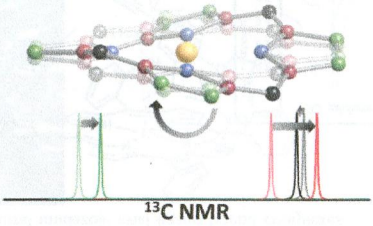

12947 dx.doi.org/10.1021/ic4012235

Structural and Magnetic Studies of a New Co(II) Thiocyanato Coordination Polymer Showing Slow Magnetic Relaxations and a Metamagnetic Transition

Susanne Wöhlert, Tomasz Fic, Zbigniew Tomkowicz, Stefan G. Ebbinghaus, Michał Rams, Wolfgang Haase, and Christian Näther*

Reaction of $Co(NCS)_2$ with 4-ethylpyridine leads to the formation of three new thiocyanato coordination compounds. In the discrete complex of composition $Co(NCS)_2(4\text{-ethylpyridine})_4$ and the dimeric compound of composition $[(Co(NCS)_2]_2(4\text{-ethylpyridine})_6$ only paramagnetic behavior is found. The 1D compound $[Co(NCS)_2(4\text{-ethylpyridine})_2]_n$ shows a metamagnetic transition. Below and above the critical field magnetic relaxations of single chains are observed. Besides this fast process there is an additional slower process which is responsible for the hysteresis loop.

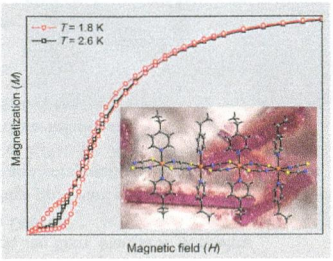

12958 dx.doi.org/10.1021/ic401291a

Selective Synthesis of Ternary Copper–Antimony Sulfide Nanocrystals

Dongying Xu, Shuling Shen, Yejun Zhang, Hongwei Gu,* and Qiangbin Wang*

The selective synthesis of high-quality ternary copper–antimony sulfide nanocrystals with diverse morphologies, compositions, and band gaps was achieved, including rectangular $CuSbS_2$ nanosheets, trigonal-pyramidal $Cu_{12}Sb_4S_{13}$ nanocrystals, and rhombic Cu_3SbS_3 nanosheets. The morphologies and compositions of copper–antimony sulfide nanocrystals were precisely controlled by simply tuning the compositions of precursors and solvents. The various band gaps of the obtained copper–antimony sulfide nanocrystals indicate their great potentials in photovoltaics and photoelectric nanodevices.

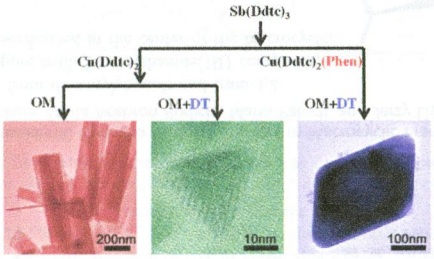

12963 Ⓢ dx.doi.org/10.1021/ic4020652

O_2 Reduction Reaction by Biologically Relevant Anionic Ligand Bound Iron Porphyrin Complexes

Subhra Samanta, Pradip Kumar Das, Sudipta Chatterjee, Kushal Sengupta, Biswajit Mondal, and Abhishek Dey*

An air stable iron porphyrin complex with an anionic thiolate axial ligand allows investigation of the details of O_2 activation by this cytochrome P450 mimic in an aqueous medium. The second-order rate of oxygen reduction reactions catalyzed by this complex are 100 times faster than neutral imidazole axial ligand bound complexes.

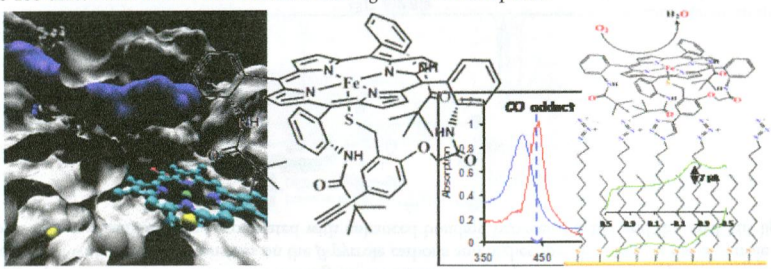

12972 Ⓢ dx.doi.org/10.1021/ic4013334

Crystal Structures and Properties of Europium Aluminum Oxynitride $Eu_2AlO_{3.75}N_{0.1}$ and Europium Aluminum Oxide $EuAl_2O_4$

Keitaro Tezuka,* Yoshimi Tokuhara, Makoto Wakeshima, Yue Jin Shan, Hideo Imoto, and Yukio Hinatsu

The reactions among Eu_2O_3, AlN, and Al_2O_3 with the ratios Eu:Al = 2:1 and 1:2 at 1200 °C for 10 h yielded $Eu_2AlO_{3.75}N_{0.1}$ and $EuAl_2O_4$, respectively. The new oxynitride $Eu_2AlO_{3.75}N_{0.1}$ has a monoclinic structure with a Ruddlesden–Popper-type structure. The photoluminescent $EuAl_2O_4$ is isostructural with $SrAl_2O_4$. The luminescence mechanism owing to $4f^7$ ($^8S_{7/2}$) ↔ $4f^65d^1$ of europium in $EuAl_2O_4$ was proposed on the basis of the calculated band structure.

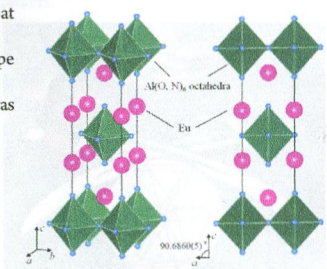

12980 Ⓢ dx.doi.org/10.1021/ic4013608

Incommensurately Modulated δ''-$Au_{1+x}Cd_{2-x}$ Formed by an Unquenchable Phase Transformation from the γ-Brass δ'-Phase

Partha P. Jana* and Sven Lidin

The structure of incommensurately modulated compound δ''-$Au_{1+x}Cd_{2-x}$ ($0.07 \leq x \leq 0.08$) is determined by single crystal X-ray diffraction measurement. The average structure shows a new structure type. The structure of the δ''-phase might be termed as a failed Frank–Kasper phase. The basic structure may be derived from that of ε-CoZn13 by crystallographic shear.

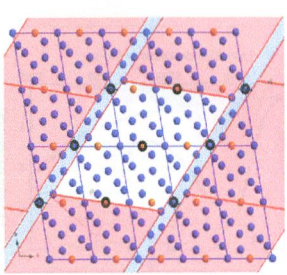

12986 Ⓢ dx.doi.org/10.1021/ic401501t

Rapid, Large-Scale, Morphology-Controllable Synthesis of YOF:Ln^{3+} (Ln = Tb, Eu, Tm, Dy, Ho, Sm) Nano-/Microstructures with Multicolor-Tunable Emission Properties

Yang Zhang, Dongling Geng, Xiaojiao Kang, Mengmeng Shang, Yuan Wu, Xuejiao Li, Hongzhou Lian, Ziyong Cheng, and Jun Lin*

Multiform YOF nano-/microstructures were fabricated via a modified urea-based homogeneous precipitation technique followed by a heat treatment. Moreover, multicolored luminescence has been successfully confected for YOF:Ln^{3+} (Ln = Tb, Eu, Tm, Dy, Ho, Sm) nanospheres.

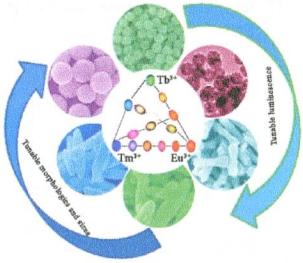

12995 Ⓢ dx.doi.org/10.1021/ic401503b

Synthesis and Characterization of *fac*-[$M(CO)_3(P)(OO)$] and *cis-trans*-[$M(CO)_2(P)_2(OO)$] Complexes (M = Re, ^{99m}Tc) with Acetylacetone and Curcumin as OO Donor Bidentate Ligands

Charalampos Triantis, Theodoros Tsotakos, Charalampos Tsoukalas, Marina Sagnou, Catherine Raptopoulou, Aris Terzis, Vassilis Psycharis, Maria Pelecanou, Ioannis Pirmettis, and Minas Papadopoulos*

The synthesis of neutral mixed ligand complexes *fac*-[$M(CO)_3(P)OO$)] and *cis-trans*-[$M(OO)(P)_2(CO)_2$] (M = Re, ^{99m}Tc), with deprotonated acetylacetone (acac) or curcumin (cur) as the OO donor bidentate ligands and a phosphine (triphenylphosphine or methyldiphenylphosphine) as the monodentate P ligand, is described. The rhenium complexes were fully characterized through IR, NMR spectroscopies and X-ray crystallography and were used as references for the characterization of their ^{99m}Tc analogues. The curcuminato complexes were successfully tested in vitro for their ability to selectively stain beta-amyloid plaques in post mortem brain slices of Alzheimer's disease patients.

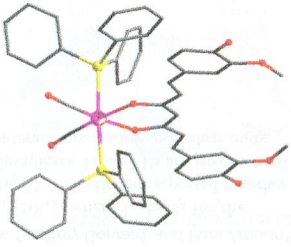

13004 Ⓢ dx.doi.org/10.1021/ic401522v

Uncorrelated Dynamical Processes in Tetranuclear Carboxylate Clusters Studied by Variable-Temperature ^1H NMR Spectroscopy.

Femke F. B. J. Janssen, Laurens C. J. M. Peters, Paul P. J. Schlebos, Jan M. M. Smits, René de Gelder, and Alan E. Rowan*

Biologically relevant tetranuclear carboxylate clusters are shown to have a complex dynamic behavior. Variable-temperature ^1H NMR studies reveal two uncorrelated exchange processes, which may play a role in their biological properties.

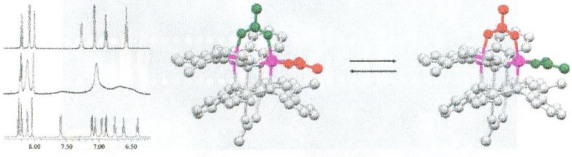

13014 S dx.doi.org/10.1021/ic401632x

Crystal Structure, Exogenous Ligand Binding, and Redox Properties of an Engineered Diiron Active Site in a Bacterial Hemerythrin

Yasunori Okamoto, Akira Onoda,* Hiroshi Sugimoto, Yu Takano, Shun Hirota, Donald M. Kurtz Jr., Yoshitsugu Shiro, and Takashi Hayashi*

A unique nonheme diiron active site containing five His and three Glu/Asp residues was constructed by replacing an adjacent Ile residue with Glu in DcrH-Hr. Direct coordination of E119 to Fe2 of the diiron site in the I119E variant was confirmed by X-ray crystallography. It is found that the modification of the endogenous coordination sphere clearly results in the pH-dependent O_2 and N^{3-} ligand bindings and the slower reduction in the nonheme diiron active site.

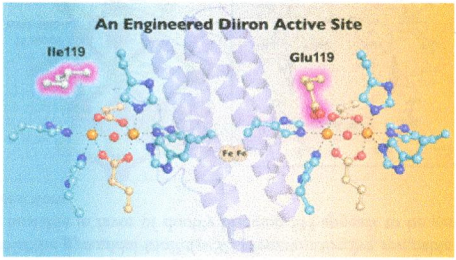

13021 S dx.doi.org/10.1021/ic401618u

Molecular and Electronic Structures of Complexes Containing 1-(2-pyridylazo)-2-phenanthrol (PAPL): Revisiting a Redox-Active Ligand

Natasha Van Damme, Alan J. Lough, Serge I. Gorelsky, and Martin T. Lemaire*

We describe the molecular structures and electronic properties of three homoleptic complexes (M^{2+} = Mn, Ni, Zn) containing the ligand 1-(2-pyridylazo)-2-phenanthrol (PAPL). Cyclic voltammetry and spectroelectrochemical experiments indicate redox-active complexes with reversible or pseudoreversible reductions that are assigned to ligand-centered processes, which produce ligand-centered radical dianions. Density funcitional theory calculations on neutral and reduced complexes support the assertion of ligand-centered redox activity.

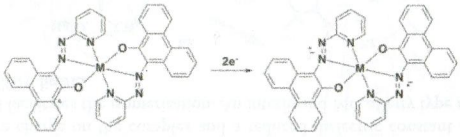

13029 Ⓢ dx.doi.org/10.1021/ic401714p

Phosphorescent Cellular Probes and Uptake Indicators Derived from Cyclometalated Iridium(III) Bipyridine Complexes Appended with a Glucose or Galactose Entity

Wendell Ho-Tin Law, Lawrence Cho-Cheung Lee, Man-Wai Louie, Hua-Wei Liu, Tim Wai-Hung Ang, and Kenneth Kam-Wing Lo*

We report a series of phosphorescent cyclometalated iridium(III) bipyridine complexes appended with a β-D-glucose moiety as new cellular probes and uptake indicators. Temperature dependence and chemical inhibition experiments indicated that the transport of bt–glucose complex **1a** across the cell membrane occurred through an energy-requiring process such as endocytosis, in addition to a pathway mediated by GLUTs. Additionally, laser-scanning confocal microscopy revealed that the complex was localized in the mitochondria and highly resistant to photobleaching.

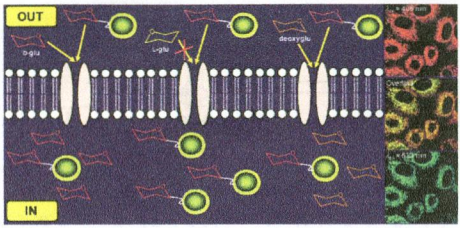

13042 Ⓢ dx.doi.org/10.1021/ic4017195

***Meso*-Helicates with Rigid Angular Tetradentate Ligand: Design, Molecular Structures, and Progress Towards Self-Assembly of Metal–Organic Nanotubes**

Rodrigue Djeda, Christophe Desmarets, Lise-Marie Chamoreau, Yanling Li, Yves Journaux, Geoffrey Gontard, and Hani Amouri*

Two novel metallosupramolecular complexes of the general formulas $[L_2M_2(CH_3CN)_4][BF_4]_4$ where L stands for the tetradentate ligand 3,5-bis[4-(2,2-dipyridylamino)phenylacetylenyl]toluene, (M = Co, **1a**; M = Ni, **1b**) are reported together with their molecular structures ascertained by single-crystal X-ray diffraction studies. Complexes **1a** and **1b** are isostructural and show the formation of dinuclear *meso*-helicates. Complex **1a** or **1b** displays π–π interactions among individual units generating a 2D network containing large cavities.

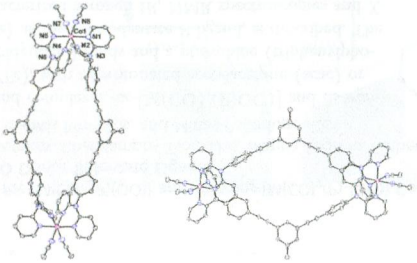

13048 Ⓢ dx.doi.org/10.1021/ic4017239

Azadipyrromethene Complexes of d^8 Metal Centers: Rhodium(I), Iridium(I), Palladium(II), and Platinum(II)

Nihal Deligonul and Thomas G. Gray*

Azadipyrromethene complexes of Rh(I), Ir(I), Pd(II), and Pt(II) have been prepared and optically characterized. New complexes bear the absorption signatures of azadipyrromethene ligands.

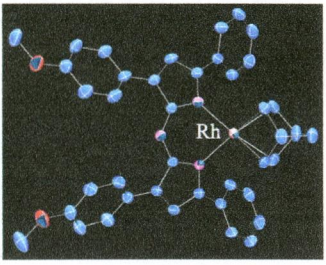

13058 Ⓢ dx.doi.org/10.1021/ic4017118

Isomerization of Platinum-Coordinated Iminoethers Induced by Spectator Ligands: Stabilization of the *Z* anti Configuration

Daniela Giardina-Papa, Francesco P. Intini, Concetta Pacifico, and Giovanni Natile*

The effect of ancillary ligands, solvent, and counterion upon the *E*−*Z* isomerization of platinum coordinated iminoethers has been investigated. A net positive charge on the complex and a reduced dielectric constant around the metal core appear to stabilize the *Z* configuration and facilitates the isomerization. An interligand McLafferty type rearrangement has been observed in the case of the thiourea ancillary ligand.

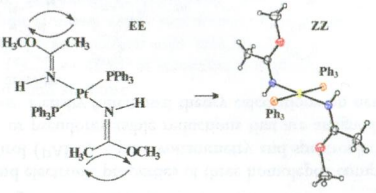

13068 dx.doi.org/10.1021/ic401818k

The Stereochemistry and Dynamics of the Introduction of Hydrogen Atoms onto FeMo-co, the Active Site of Nitrogenase

Ian Dance*

DFT calculations show that protonation of triply bridging sulfide (S3B) in FeMo-co generates a doubly bridging SH ligand and that configurational changes in the pyramidal MoFe(μ-SH) function involve reversible elongations of Fe−S bonds. The result that triply bridging SH is unstable in favor of doubly bridging SH appears to be general, with implications for other metal sulfide clusters and their reactions.

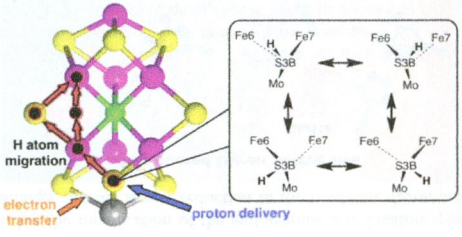

13078 S dx.doi.org/10.1021/ic4019025

Pentanuclear Heterometallic {Ni_2Ln_3} (Ln = Gd, Dy, Tb, Ho) Assemblies. Single-Molecule Magnet Behavior and Multistep Relaxation in the Dysprosium Derivative

Vadapalli Chandrasekhar,* Prasenjit Bag, Wolfgang Kroener, Klaus Gieb, and Paul Müller

Magnetic measurements on the pentanuclear heterometallic complex $Ni_2Dy_3(LH)_4]Cl{\cdot}3CH_3OH$ reveal that it shows the highest effective energy barrier, U_{eff} = 85 K, for magnetization reversal among all the Ni^{II}/Ln^{III} complexes reported so far. This compound also shows an open hysteresis loop up to 3 K at a sweep rate 50 mT/s.

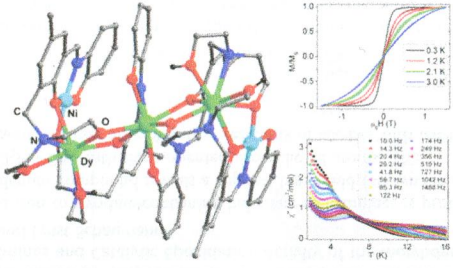

13087 dx.doi.org/10.1021/ic401943r

A Rapid Microwave-Assisted Solvothermal Approach to Lower-Valent Transition Metal Oxides

Zachary Moorhead-Rosenberg, Katharine L. Harrison, Travis Turner, and Arumugam Manthiram*

A green, rapid microwave-assisted solvothermal process using tetraethylene glycol (TEG) as a reducing agent has been explored as a soft-chemistry route for the preparation of various lower-valent binary and ternary transition metal oxides. In comparison to traditional hydrogen gas reduction of higher-valent oxides, the method described here is much faster, safer, and more energy efficient. The products have been characterized by X-ray powder diffraction and iodometric titration.

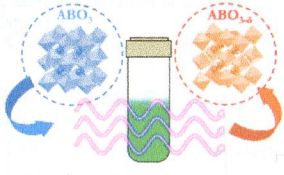

13094 S dx.doi.org/10.1021/ic4019713

γ-Brass Polyhedral Core in Intermetallics: The Nanocluster Model

Arina A. Pankova, Vladislav A. Blatov,* Gregory D. Ilyushin, and Davide M. Proserpio*

Using the TOPOS program package, 26-atom nanoclusters of the γ-brass (Cu_5Zn_8) type (0@4@22 or 0@8@18) were found in 5918 crystal structures of cubic intermetallics. It is shown that the 0@4@22 nanoclusters frequently occur as building units of intermetallics of different composition and structure type. Regularities in chemical composition of 702 γ-brass-type nanoclusters were found within both the nanoclusters approach (multishell structure) and the nested-polyhedra model. A database containing all topological types of γ-brass nanoclusters is created.

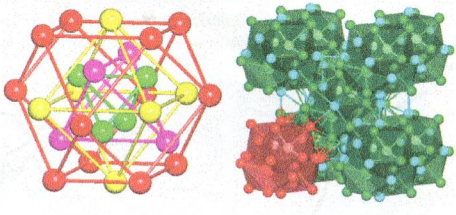

13108 dx.doi.org/10.1021/ic401994m

Synthesis and Isolation of Methacrylate- and Acrylate-Functionalized Polyhedral Oligomeric Silsesquioxanes (T_8, T_{10}, and T_{12}) and Characterization of the Relationship between Their Chemical Structures and Physical Properties

Vuthichai Ervithayasuporn* and Supansa Chimjarn

Organic–inorganic hybrid nanobuilding blocks of methacrylate- and acrylate-functionalized polyhedral oligomeric silsesquioxanes (T_8, T_{10}, and T_{12}) were easily prepared and separated in their pure forms. Octakis(3-propyl methacrylate)-octasilsesquioxane (T_8) is a colorless, crystalline solid with a melting point of 66.7-67.2 °C, while the other cage products are colorless viscous liquids at room temperature.

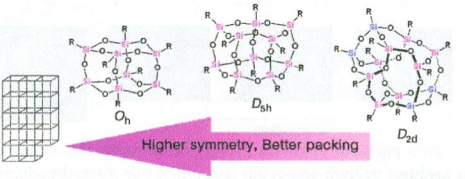

13113 dx.doi.org/10.1021/ic402001t

Cu^{I} Thiolate Reactivity with Dioxygen: The Formation of Cu^{II} Sulfinate and Cu^{II} Sulfonate Species via a Cu^{II} Thiolate Intermediate

Erica C.M. Ording-Wenker, Maxime A. Siegler, Martin Lutz, and Elisabeth Bouwman*

A new Cu^{I} thiolate complex that is oxidized by dioxygen from air was studied. It was found that the oxidation goes via a dinuclear Cu^{II} thiolate intermediate, which bears similarity to the Cu_A active site, to form Cu^{II} sulfinate and Cu^{II} sulfonate complexes, providing a model for the oxidative degeneration of copper–sulfur enzymes. The Cu^{II} sulfinate and Cu^{II} sulfonate complexes were isolated and studied.

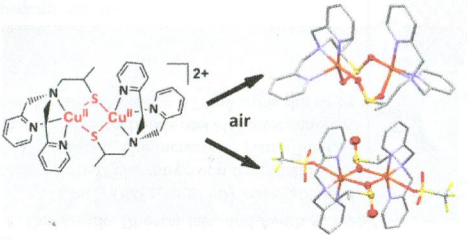

13123 dx.doi.org/10.1021/ic402013n

Mössbauer Spectroscopy as a Probe of Magnetization Dynamics in the Linear Iron(I) and Iron(II) Complexes $[Fe(C(SiMe_3)_3)_2]^{1-/0}$

Joseph M. Zadrozny,* Dianne J. Xiao, Jeffrey R. Long,* Mihail Atanasov,* Frank Neese,* Fernande Grandjean,* and Gary J. Long*

Mössbauer spectroscopy is used to determine the magnetization dynamics of $[K(crypt\text{-}222)][Fe(C(SiMe_3)_3)_2]$, **1**, and $Fe(C(SiMe_3)_3)_2$, **2**, dynamics that include the relaxation mechanism of **1** at high temperatures and of **2** in a zero applied dc field, mechanisms that can not be obtained by conventional magnetometry. The high-temperature regime reveals Orbach relaxation processes with U_{eff} = 246(3) and 178(9) cm^{-1} for **1** and **2**, respectively, effective relaxation barriers that are in agreement with magnetic measurements and supporting ab initio calculations.

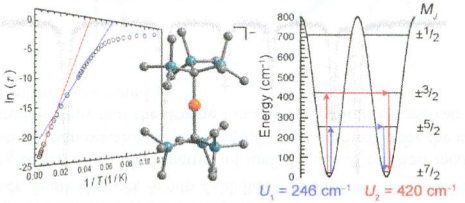

13132 S dx.doi.org/10.1021/ic402027j

Sugar–Metal Ion Interactions: The Complicated Coordination Structures of Cesium Ion with D-Ribose and *myo*-Inositol

Haijian Hu, Junhui Xue, Xiaodong Wen, Weihong Li, Chao Zhang, Limin Yang,* Yizhuang Xu,* Guozhong Zhao, Xiaoxia Bu, Kexin Liu, Jia'er Chen, and Jinguang Wu

The novel cesium chloride–D-ribose complex ($CsCl{\cdot}C_5H_{10}O_5$; Cs-R) and cesium chloride–*myo*-inositol complex ($CsCl{\cdot}C_6H_{12}O_6$; Cs-I) were synthesized and characterized using X-ray diffraction and FTIR, FIR, THz, and Raman spectroscopy.

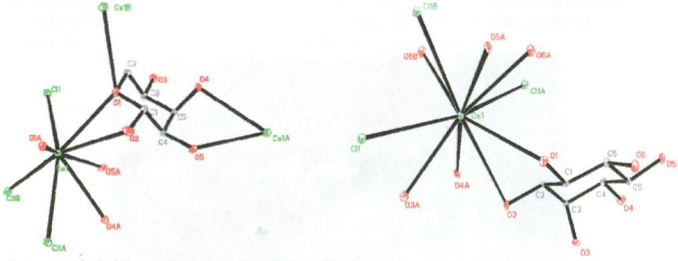

13146 S dx.doi.org/10.1021/ic402059b

Theoretical Study of Mononuclear Nickel(I), Nickel(0), Copper(I), and Cobalt(I) Dioxygen Complexes: New Insight into Differences and Similarities in Geometry and Bonding Nature

Yue Chen and Shigeyoshi Sakaki*

The transition-metal dioxygen complexes (N^N)M(O_2) (M = Co, Ni, and Cu; N^N = β-diketiminate) and $(Ph_3P)_2Ni(O_2)$ were investigated by DFT and MS-RASPT2 methods. All these complexes exhibit superoxo (O_2^-) character. The M–O distance, the interaction energy of O_2 with metal, and the reactivity for hydrogen abstraction reaction depend on the d_π orbital energy in the valence state.

13160 S dx.doi.org/10.1021/ic4020306

Synthesis and Structural Characterization of Molybdenum(VI) and Iron(II) Coordination Compounds with *S*-Alkyl-*N*-methyl-*S*-(2-pyridyl)sulfoximines and Catalytic Epoxidation Activity of the Molybdenum Complexes

Yvonne Brussaard, Falk Olbrich, and Ernst Schaumann*

The binding of molybdenum and iron to pyridine-containing bidentate sulfoximines is probed. The crystal structure of a molybdenum compound reveals a trigonal bipyramid (shown) and for an iron compound a planar μ^2-Cl_2Fe_2 ring with trans-oriented exocyclic Cl atoms. The molybdenum complexes are efficient catalysts in epoxidation reactions of alkenes with *tert*-butyl hydroperoxide.

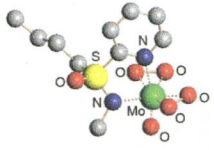

13167 S dx.doi.org/10.1021/ic4020724

Coordination of Terpyridine to Li^+ in Two Different Ionic Liquids

Klaus Pokorny, Matthias Schmeisser, Frank Hampel, Achim Zahl, Ralph Puchta, and Rudi van Eldik*

To achieve a better understanding of the role and properties of ionic liquids as reaction media, detailed ^7Li NMR and structural studies on the complex-formation reaction of $[Li(terpy)_2]^+$ were performed for the ionic liquids $[emim][NTf_2]$ and $[emim][ClO_4]$ as solvents. The studies show that the driving force of a chemical process can significantly be affected by the nature of the anionic component of the ionic liquid.

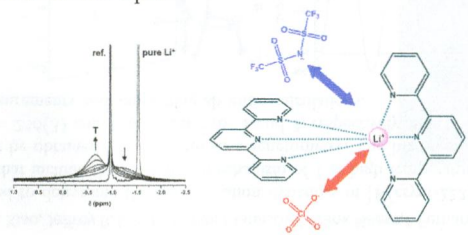

13179 S dx.doi.org/10.1021/ic402085w

Synthesis and Structural and Electrical Investigations of a Hexagonal $Y_{1-x}Gd_xInO_3$ ($0.0 \leq x \leq 1.0$) System Obtained via Metastable C-Type Intermediates

Rakesh Shukla, Vinita Grover,* S. K. Deshpande, Dheeraj Jain, and Avesh K. Tyagi*

The A-site disordered hexagonal $Y_{1-x}Gd_xInO_3$ ($0.0 \leq x \leq 1.0$) series obtained via metastable C-type phase has been explored. The conversion temperature (C-type to hexagonal) increased with Y^{3+} content. The increase in planar In−O bonds (InO_5 polyhedra) is twice that of the apical bonds on Gd^{3+} substitution. A subtle definitive structural change in the lattice from $x = 0.7$ onward is shown by Raman and dielectric studies.

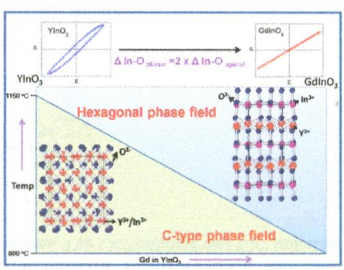

13188 S dx.doi.org/10.1021/ic402104q

Photo- and Vapor-Controlled Luminescence of Rhombic Dicopper(I) Complexes Containing Dimethyl Sulfoxide

Atsushi Kobayashi, Kahori Komatsu, Hiroki Ohara, Waka Kamada, Yuko Chishina, Kiyoshi Tsuge, Ho-Chol Chang, and Masako Kato*

We synthesized novel halide-bridged rhombic dicopper(I) complexes, $[Cu_2(\mu\text{-}X)_2(DMSO)_2(PPh_3)_2]$ (X = I^-, Br^-; DMSO = dimethyl sulfoxide; PPh_3 = triphenylphosphine), and found that the iodide-bridged complex shows interesting photochromic luminescence driven by photoirradiation and exposure to DMSO vapors in the solid state.

13199 S dx.doi.org/10.1021/ic4021542

Determination of Crystal-Field Energy Levels and Temperature Dependence of Magnetic Susceptibility for Dy^{3+} in $[Dy_2Pd]$ Heterometallic Complex

Mirosław Karbowiak,* Czesław Rudowicz, and Takayuki Ishida

Heterometallic 4f-3d compounds are intensively studied for the development of novel single-molecule magnets. In this paper experimental energy levels of Dy^{3+} ions in the powder $[\{Dy^{III}(hfac)_3\}_2Pd^{II}(dpk)_2]$ sample were determined from absorption spectra, and crystal-field analysis was performed yielding the energies and exact composition of the state vector for the ground multiplet $^6H_{15/2}$ of Dy^{3+}. These results are used for the simulation of the temperature dependence of the magnetic susceptibility, which enables a theoretical interpretation of the experimentally measured magnetic susceptibility.

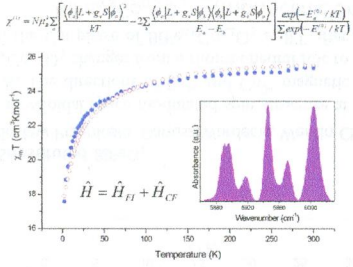

13207 S dx.doi.org/10.1021/ic402162d

Structures and Stability of Molecular $InBr_3Py_x$ (x = 1−3) Complexes: Unexpected Solid State Stabilization of Dimeric $In_2Br_6Py_4$ As Compared to Valence-Isoelectronic Group 15 and 17 Halogen Bridging Dimers

Igor V. Kazakov, Michael Bodensteiner, Anna S. Lisovenko, Andrew V. Suvorov, Manfred Scheer, Gábor Balázs, and Alexey Y. Timoshkin*

Although metastable $In_2Br_6Py_4$ has been structurally characterized in the solid state, its more stable group 17 and 15 valence-isoelectronic halogen bridging dimers are still unknown.

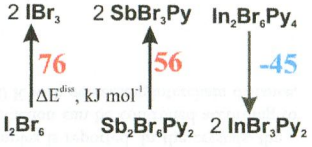

13216 S dx.doi.org/10.1021/ic402130p

Chloro- and Trifluoromethyl-Substituted Flanking-Ring *m*-Terphenyl Isocyanides: η^6-Arene Binding to Zero-Valent Molybdenum Centers and Comparison to Alkyl-Substituted Derivatives

Treffly B. Ditri, Alex E. Carpenter, Donald S. Ripatti, Curtis E. Moore, Arnold. L. Rheingold, and Joshua S. Figueroa*

To combat the formation flanking-ring, η^6-arene interactions to low-valent metal centers, new *m*-terphenyl isocyanide derivatives featuring electron-withdrawing substituents have been prepared. The coordination chemistry of these new ligands has been examined and compared with that of more-traditional, alkyl-substituted *m*-terphenyl isocyanides. These ligands expand the library of *m*-terphenyl isocyanides and offer new steric and electronic environments for low-valent metal complexes.

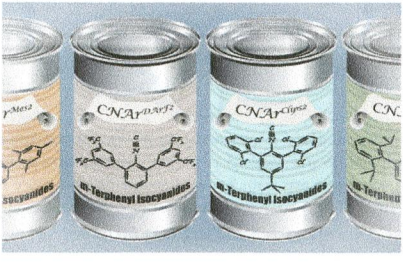

13230 Ⓢ dx.doi.org/10.1021/ic4021838

Mixed-Spin [2 × 2] Fe_4 Grid Complex Optimized for Quantum Cellular Automata

Benjamin Schneider, Serhiy Demeshko, Sven Neudeck, Sebastian Dechert, and Franc Meyer*

The new pyrazolate-bridged proligand 4-methyl-3,5-bis{6-(2,2′-bipyridyl)}pyrazole (^{Me}LH) has been synthesized. Similar to its congener that lacks the backbone methyl substituent (^{H}LH) it forms a robust Fe^{II}_4 grid complex, $[^{Me}L_4Fe^{II}_4](BF_4)_4$. The molecular structure of $[^{Me}L_4Fe^{II}_4](BF_4)_4 \cdot 2MeCN$ has been elucidated by X-ray diffraction, revealing two high-spin (HS) and two low-spin (LS) ferrous ions at opposite corners of the rhombic metal ion arrangement.

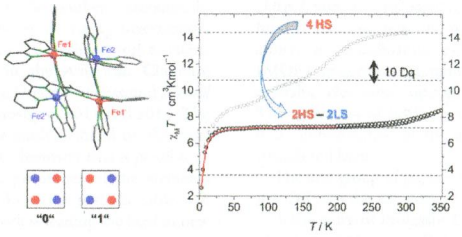

13238 dx.doi.org/10.1021/ic402189c

Various Three-Dimensional Structures Connected by Al–O/OH/Acetate–Al Bonds

Katalin Sinkó,* Shiro Kubuki, and Herwig Peterlik

A novel fast, low energy and cost consumption sol–gel technique has been evolved for preparation of various structures connected by Al–O/OH/acetate–Al bonds: nanofibrous, macroporous, hierarchical porous, and compact systems. The shared OH and acetate ions as bidentate ligands provide the spinnability. The octahedral Al(III) ions are connected by OH/O-bridges in the highly porous materials. The bond systems of monoliths with low porosity can be characterized by O-bridges between tetra-, octa-, and pentahedrally coordinated Al(III) ions.

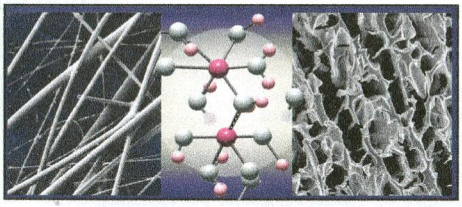

13244 Ⓢ dx.doi.org/10.1021/ic402188x

Defect Structure, Phase Separation, and Electrical Properties of Nonstoichiometric Tetragonal Tungsten Bronze $Ba_{0.5-x}TaO_{3-x}$

Xiaojun Kuang,* Fengjuan Pan, Jiang Cao, Chaolun Liang, Matthew R. Suchomel, Florence Porcher, and Mathieu Allix*

The highly nonstoichiometric TTB $Ba_{0.5-x}TaO_{3-x}$, showing Ba^{2+} migration, contains distinct Ba^{2+} chains and alternation of Ta and O rows in the pentagonal tunnels. The slight nonstoichiometry in $Ba_{0.5-x}TaO_{3-x}$ leads to framework oxygen and tunnel cation deficiencies. Phase separation into two closely related $(TaO)^{3+}$-free and $(TaO)^{3+}$-containing TTB phases occurs for intermediate compositions.

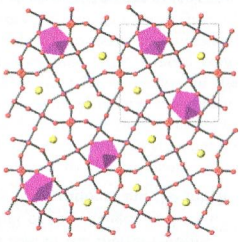

13253 S dx.doi.org/10.1021/ic402207u

Anion Encapsulation and Geometric Changes in Hepta- and Hexanuclear Copper(I) Dichalcogeno Clusters: A Theoretical and Experimental Investigation

Camille Latouche, Samia Kahlal, Yan-Ru Lin, Jian-Hong Liao, Eric Furet, C. W. Liu,* and Jean-Yves Saillard*

Calculations indicate that hepta- and hexanuclear Cu(I) clusters of the type $[Cu^I]_n(E^{\cap}E)_6$ (n = 7, 6; $E^{\cap}E$ = dithio or diseleno ligand) can encapsulate an hydride or a main-group anion, adapting their size and shape to the size and electronic demand of their host. Experimental X-ray structures of previously published clusters and of new halide-containing species confirm the theoretical results and support the prediction for the so far hypothetical compounds.

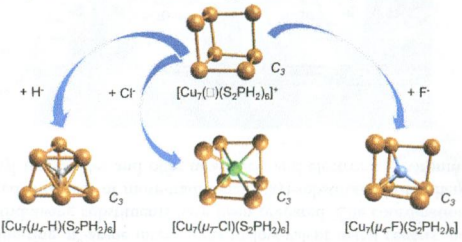

13263 S dx.doi.org/10.1021/ic402217c

A Series of Weak Ferromagnets Based on a Chromium–Acetylide–TTF Type Complex: Correlation of the Structures and Magnetic Properties and Origin of the Weak Ferromagnetism

Junichi Nishijo* and Masaya Enomoto

A new series of weak ferromagnets containing a chromium–acetylide–TTF type complex is reported. In the crystals, the acetylide complexes form ferrimagnetic chains and the strength of the interchain interaction can be controlled according to solvent and anion substitutions. The transition temperature increases from 14.5 to 26.0 K with decreasing interchain distance, while the remanent magnetization at 2 K decreases from 0.0215 to 0.0079 μ_B.

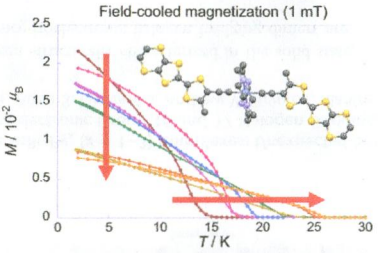

13269 S dx.doi.org/10.1021/ic402427q

Crystal and Magnetic Structure in Co-Substituted $BiFeO_3$

Izabela Sosnowska,* Masaki Azuma, Radosław Przeniosło, Dariusz Wardecki, Wei-tin Chen, Kengo Oka, and Yuichi Shimakawa

$BiFe_{0.8}Co_{0.2}O_3$ shows a transition from a cycloidal space modulated spin structure at T = 10 K to a collinear G-type antiferromagnetic structure at T = 120 K. The directions of Fe^{3+} and Co^{3+} magnetic moments are antiparallel. On heating above RT, the crystal structure of $BiFe_{0.8}Co_{0.2}O_3$ changes from a rhombohedral $R3c$ to a monoclinic Cm. The collinear C-type antiferromagnetic structure is present in the Cm phase of $BiFe_{0.8}Co_{0.2}O_3$ at RT after annealing.

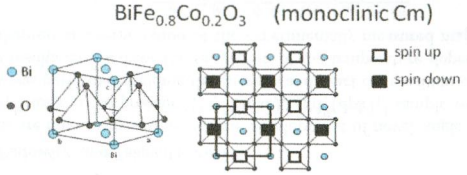

13278 Ⓢ dx.doi.org/10.1021/ic402432q

Thermochromism, the Alexandrite Effect, and Dynamic Jahn–Teller Distortions in $Ho_2Cu(TeO_3)_2(SO_4)_2$

Jian Lin, Kariem Diefenbach, Justin N. Cross, Jean-Marie Babo, and Thomas E. Albrecht-Schmitt*

The 3d–4f heterobimetallic material, $Ho_2Cu(TeO_3)_2(SO_4)_2$, exhibits both thermochromism and the Alexandrite effect. Variable temperature single crystal X-ray diffraction and UV–vis-NIR spectroscopy reveal that changes in the Cu^{II} coordination geometry result in negative thermal expansion of axial Cu–O bonds that plays a role in the thermochromic transition of $Ho_2Cu(TeO_3)_2(SO_4)_2$. However, the thermochromic transition is not solely a result of the changes in the Cu^{II} coordination environment but rather a subtle interplay between the sharp f–f transitions of the Ho^{III} cations, and the much broader Cu^{II} transitions are responsible for the pink to green transition.

13282 Ⓢ dx.doi.org/10.1021/ic402626p

1,4,7-Triazacyclononane Ligands Bearing Tertiary Alkyl Nitrogen Substituents

Arumugam Thangavel, Marika Wieliczko, John Bacsa, and Christopher C. Scarborough*

The first derivatives of the classic ligand 1,4,7-triazacyclononane (H_3tacn) bearing tertiary alkyl nitrogen substituents, $^tBu_3tacn$ and Ad_3tacn, are described along with their first-row transition-metal coordination compounds. $^tBu_3tacn$ and Ad_3tacn are significantly bulkier than all previous R_3tacn derivatives and enforce the lowest coordination numbers observed for R_3tacn compounds of Cr^{II}, Mn^{II}, Fe^{II}, Co^{II}, and Ni^{II}.

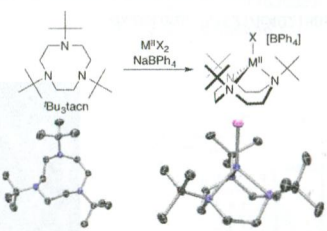

Additions and Corrections

13288 dx.doi.org/10.1021/ic402722x

Correction to New Iron(II) Spin Crossover Coordination Polymers $[Fe(\mu\text{-atrz})_3]X_2\cdot 2H_2O$ ($X = ClO_4^-$, BF_4^-) and $[Fe(\mu\text{-atrz})(\mu\text{-pyz})(NCS)_2]\cdot 4H_2O$ with an Interesting Solvent Effect

Yu-Chun Chuang, Chi-Tsun Liu, Chou-Fu Sheu, Wei-Lun Ho, Gene-Hsiang Lee, Chih-Chieh Wang, and Yu Wang*

Ⓢ Supporting Information available via online article